Medical Radiology · Radiation Oncology
Series Editors: L.W. Brady · S.E. Combs · J.J. Lu

Hans Geinitz
Mack Roach III
Nicholas van As *Editors*

Radiotherapy in Prostate Cancer

Innovative Techniques and Current Controversies

Springer

Medical Radiology

Radiation Oncology

Series editors

Luther W. Brady
Stephanie E. Combs
Jiade J. Lu

For further volumes:
http://www.springer.com/series/4353

Hans Geinitz · Mack Roach III
Nicholas van As
Editors

Radiotherapy in Prostate Cancer

Innovative Techniques and Current Controversies

Springer

Editors
Hans Geinitz
Department of Radiation Oncology
Krankenhaus der Barmherzigen
Schwestern Linz
Medical Faculty, Johannes Kepler University
Linz
Austria

Mack Roach III
Department of Radiation Oncology
University of California
San Francisco, CA
USA

Nicholas van As
The Institute of Cancer Research
Sutton Surrey
UK

ISSN 0942-5373 ISSN 2197-4187 (electronic)
ISBN 978-3-642-37098-4 ISBN 978-3-642-37099-1 (eBook)
DOI 10.1007/978-3-642-37099-1
Springer Heidelberg New York Dordrecht London

Library of Congress Control Number: 2014953516

For Anja, Nora, Thilo and Vera
Hans Geinitz

Acknowledgments

We would like to thank all the authors who contributed enthusiastically to the completion of this book. While editing the volume we ourselves got new insights and different angles on how to see and practice prostate radiation oncology. Beyond its content, the book is a virtuous example for a fruitful international cooperation embracing Europe and North America.

Linz, October 2014 — Hans Geinitz
San Francisco — Mack Roach III
Sutton — Nicholas van As

Contents

Contributors

Nicolaus Andratschke Department of Radiation Oncology, University Hospital Zurich, Zürich, Switzerland

Giorgio Arcangeli Regina Elena National Cancer Institute, Rome, Italy

Stefano Arcangeli Regina Elena National Cancer Institute, Rome, Italy

Claus Belka Department of Radiation Oncology, Ludwig-Maximilians-University (LMU), Munich, Germany

Dirk Böhmer Department of Radiation Oncology, Charité University Medicine, Berlin, Germany

Michel Bolla Clinique Universitaire de Cancérologie-Radiothérapie, Centre Hospitalier Universitaire Albert Michallon, Grenoble, France

Dirk Bottke Department of Radiotherapy and Radiation Oncology, University Hospital Ulm, Ulm, Germany

Violaine Brun Baronnat Clinique Universitaire de Cancérologie-Radiothérapie, Centre Hospitalier Universitaire Albert Michallon, Grenoble, France

Wilfried Budach Medical Faculty, Department of Radiation Oncology, Heinrich Heine University of Düsseldorf, Düsseldorf, Germany

Jürgen Debus Radiologische Universitätsklinik, Strahlenklinik, Heidelberg, Germany

Georges Decker Department of Radiology, University of Bonn, Bonn, Germany

Marciana Nona Duma Department of Radiation Oncology, Klinikum rechts der Isar, Technische Universität München, München, Germany

Ute Ganswindt Department of Radiation Oncology, Ludwig-Maximilians-University (LMU), Munich, Germany

Michael Geier Department of Radiation Oncology, Krankenhaus der Barmherzigen Schwestern Linz, Linz, Austria

Hans Geinitz Department of Radiation Oncology, Krankenhaus der Barmherzigen Schwestern Linz, Medical Faculty, Johannes Kepler University, Linz, Austria

Pirus Ghadjar Department of Radiation Oncology, Inselspital, Bern University Hospital, Bern, Switzerland

Gregor Goldner Klinik für Strahlentherapie, MUW Wien, Allgemeines Krankenhaus, Wien, Austria

A. L. Grosu Department of Radiation Oncology, Medical University of Freiburg, Freiburg, Germany

Arne Grün Department for Radiation Oncology and Cyberknife Cente, Charité—University Medicine Berlin Campus Virchow-Clinic, Berlin, Germany

Jürgen E. Gschwend Department of Urology, Klinikum rechts der Isar, Technische Universität München, Munich, Germany

Matthias Guckenberger Department of Radiation Oncology, University Hospital Zurich (USZ), Zurich, Switzerland

Gregor Habl Radiologische Universitätsklinik, Strahlenklinik, Heidelberg, Germany

Daniel Robert Henderson Clinical Oncology Royal Marsden Hospital London, London, UK

Thomas Horn Department of Urology, Klinikum rechts der Isar, Technische Universität München, Munich, Germany

Mitchell Kamrava Department of Radiation Oncology, University of California Los Angeles, Los Angeles, CA, US

Marisa A. Kollmeier Department of Radiation Oncology, Memorial Sloan-Kettering Cancer Center, New York, NY, USA

Hubert Kübler Department of Urology, Klinikum rechts der Isar, Technische Universität München, Munich, Germany

Patrick Kupelian Department of Radiation Oncology, University of California Los Angeles, Los Angeles, CA, US

Tanja Langsenlehner Department of Therapeutic Radiology and Oncology, Medical University of Graz, Graz, Austria

Wolfgang Lilleby MD Anderson, Norwegian Cancer Consortium (NCC), Oncology, Oslo, Norway

Tobias Maurer Department of Urology, Klinikum rechts der Isar, Technische Universität München, Munich, Germany

Alexandros Papachristofilou Department of Radiation Oncology, University Hospital Basel, Basel, Switzerland

Pascal Pommier Radiotherapy Department, Centre Léon Bérard, Lyon, France

H. C. Rischke Department of Radiation Oncology, Medical University of Freiburg, Freiburg, Germany; Department of Nuclear Medicine, Medical University of Freiburg, Freiburg, Germany

Mack Roach III Department of Radiation Oncology, Helen Diller Family Comprehensive Cancer Center, University of California San Francisco (UCSF), San Francisco, CA, USA

Irina Sackerer Department of Radiation Oncology, Klinikum rechts der Isar, Technische Universität München, Munich, Germany

Ralf A. Schneider Center for Proton Therapy, Paul Scherrer Institute, Villigen, Switzerland

Lidia Strigari Regina Elena National Cancer Institute, Rome, Italy

Martin Stuschke Direktor der Klinik und Poliklinik für Strahlentherapie, Universitätsklinikum Essen, Essen, Germany

Alexandre Tessier Clinique Universitaire de Cancérologie-Radiothérapie, Centre Hospitalier Universitaire Albert Michallon, Grenoble, France

Reinhard Thamm Department of Radiation Oncology, University of Ulm, Ulm, Germany

Frank Träber Department of Radiology, University of Bonn, Bonn, Germany

Klaus-Rüdiger Trott Department of Oncology, University College London, London, UK

Nikolaos Tselis Sana Klinikum Offenbach Strahlenklinik, Offenbach, Germany

Nicholas van As The Royal Marsden Hospital, London, UK

Camille Verry Clinique Universitaire de Cancérologie-Radiothérapie, Centre Hospitalier Universitaire Albert Michallon, Grenoble, France

Thomas Wiegel Klinik für Strahlentherapie und Radioonkologie, Universitätsklinikum Ulm, Ulm, Germany

Winfried A. Willinek Department of Radiology, University of Bonn, Bonn, Germany

Nikolaos Zamboglou Sana Klinikum Offenbach Strahlenklinik, Offenbach, Germany

Michael J. Zelefsky Department of Radiation Oncology, Memorial Sloan-Kettering Cancer Center, New York, NY, USA

Frank Zimmermann Department of Radiation Oncology, University Hospital Basel, Basel, Switzerland

Part I

Imaging, Delineation and Immobilization

MR Imaging and MR Spectroscopy in Prostate Cancer

Winfried A. Willinek, Georges Decker, and Frank Träber

Contents

Abstract

Multiparametric MR Imaging with high resolution T2-weighted imaging (HR-T2WI), diffusion weighted imaging (DWI), dynamic contrast enhanced MRI (DCE-MRI), and MR spectroscopy (MRS) plays a crucial role in the assessment, localization, staging, biopsy planning, and therapy monitoring of prostate cancer (PCa) through delivering unmatched soft tissue contrast as well as functional information especially regarding cell density, vascularization, and metabolism. It also helps identifying tumors missed on PSA testing, DRE, and TRUS-guided biopsy. HR-T2WI provides a clear depiction of the prostate zonal anatomy and is indispensable for PCa detection, localization, and accurate tumor staging. DWI adds information about cellular density by quantifying Brownian motion of interstitial water molecules and thereby enabling the differentiation of benign from malignant tissue. DCE-MRI is another functional imaging technique which allows for characterizing pharmacokinetic features reflecting the prostatic vascularization through a series of high temporal resolution T1-weighted images following the administration of contrast medium. In-vivo proton MRS investigates the biochemical constituents of prostate tissue noninvasively. Metabolic alterations caused by cancerous infiltration can be identified as well as metabolic response in the course of radiotherapy. While in the healthy gland citrate provides the predominant signal in MR spectra, strong accumulation of choline compounds indicates PCa, and the choline/citrate ratio may serve as suitable biomarker for malignancy. MRS allows simultaneous acquisition of spatially localized spectra from a multitude of tissue volumes as small as 1 cm^3 or below, with complete prostate coverage.

W.A. Willinek (✉) · G. Decker · F. Träber
Department of Radiology, University of Bonn,
Sigmund-Freud-Str. 25, 53105 Bonn, Germany
e-mail: Winfried.Willinek@ukb.uni-bonn.de

H. Geinitz et al. (eds.), *Radiotherapy in Prostate Cancer*, Medical Radiology. Radiation Oncology,
DOI: 10.1007/174_2014_1034, © Springer-Verlag Berlin Heidelberg 2014
Published Online: 4 September 2014

1 The Role of Magnetic Resonance Imaging (MRI) in the Diagnosis and Therapy Monitoring of Prostate Cancer (PCa)

The diagnosis of prostate cancer (PCa) is mainly based on prostate-specific antigen (PSA) testing, digital rectal examination (DRE), and transrectal ultrasonography (TRUS) with optional TRUS-guided biopsy. All these tests have relevant limitations. PSA testing has a low specificity because some conditions such as infections or benign prostatic hyperplasia (BPH) can also induce PSA elevation (Romero Otero et al. 2014). Furthermore, some studies suggest that PSA testing does not provide an accurate surrogate measure of cancer cure or treatment efficacy up to the first 4–5 years after radiation therapy (Vicini et al. 2005). DRE only allows the posterior surface of the gland to be palpated and neither offers high specificity nor sensitivity nor is it suitable for therapy monitoring.

In case of a suspicious PSA or DRE result, initially a TRUS-guided sextant biopsy with acquisition of 12 cores minimum is recommended to be performed. Unfortunately, TRUS biopsy is prone to underestimating the prevalence and aggressiveness of the disease: about 35 % of PCas are missed by the first biopsy (Djavan et al. 2001) and the highest Gleason score is missed in about 46 % of cases (Noguchi et al. 2001). This often leads to insufficient diagnoses, inaccurate risk assessments, and ultimately a less-than-optimal therapy. Furthermore, patients with understaged PCa may undergo radical surgery without prognostic benefits.

About 15 % of PCa patients have normal PSA levels, and no tumor is palpable in DRE. Unfortunately, among these clinically silent tumors, about 15.6 % have a Gleason score ranging from 7 to 9 (Thompson et al. 2004). Recent studies reported a sensitivity and specificity by MRI of 84.2 and 66.6% respectively in the detection of clinically low-risk PCa with Gleason scores less than or equal to 6. In contrast, cancers with higher Gleason grades, i.e., clinically significant tumors, had a detection accuracy of about 90 % (Kim et al. 2014) and a negative predictive value of up to 95 % (Arumainayagam et al. 2013). Other research groups found diffusion-weighted imaging (DWI) at 3 Tesla (T) alone detecting significant PCa with a sensitivity and specificity ranging from 89 to 91 % and 77 to 81 %, respectively (Bains et al. 2014). These data enhance the important role of MRI in detecting those PCas that need more radical treatments.

Among imaging modalities, MRI is unmatched regarding the morphologic and functional evaluation of the prostate gland (Delongchamps et al. 2011). Computed tomography (CT) does not provide sufficient tissue contrast discrimination in the prostate. However, it is valuable in the assessment of pelvic lymph nodes and bone metastases, although MRI has been shown to be superior here too (Dotan 2008). A recent study with 922 patients who received prostate multiparametric MRI (mp-MRI) before radical prostatectomy reported a detection accuracy of 91 % for lymph node metastases with a negative prediction value of 94.5 % (Jeong et al. 2013).

MRI can not only help identifying tumors missed on PSA testing, DRE, and TRUS-guided biopsy but also increases biopsy yields if performed before biopsy through prior localization. This holds true especially in the anterior parts of the prostate gland, which are typically only difficult to reach by standard TRUS.

In the perspective of the above-mentioned limitations of PSA, DRE, and TRUS, MRI represents an attractive imaging modality with high spatial resolution and excellent soft tissue contrast. For many PCa patients, MRI is currently the only modality to delineate potentially malignant foci. In consequence, MRI of the prostate is increasingly used for detection and localization of PCa including consecutive radiation therapy and radiation boost planning.

Assessment of radiation therapy effectiveness, tumor recurrence, and therapy monitoring in PCa is still a challenge. Local recurrence of PCa is actually diagnosed by PSA kinetics. Unfortunately, patterns of PSA kinetics cannot conclusively differentiate between local therapy failure and distant metastasis (Roach et al. 2006). DRE is difficult to interpret during and after radiation therapy, due to associated effects such as induced fibrosis. MRI and especially DWI can reflect cellular changes in malignant tissue under radiotherapy (Song et al. 2010). With the recent technical advancements in MRI, preliminary studies showed that DWI plays an important role in detecting PCa recurrence after radiation therapy (Kim et al. 2009). Mp-MRI can also be useful in the planning of radiation therapy by providing important information for determination of the radiation boost and coverage (Chang et al. 2014).

With the increasing availability of 3T MR systems, MRI of PCa has dramatically improved. Most functional techniques in mp-MRI benefit when moving from 1.5 to 3 T (Lagemaat and Scheenen 2014). The intrinsic signal-to-noise gain at 3 T allows for replacement of the endorectal coil by phased-array coils which enhances patient comfort and compliance. In the future, combined MR-PET may add further molecular targets to the multiparametric information that is provided already today. However, published data are still limited, and further studies are necessary to establish the clinical role of hybrid imaging in PCa.

Over all, according to the authors' opinion, state-of-the-art MR imaging is indispensable in the modern, interdisciplinary work-up of PCa prioritizing T2-weighted and diffusion-weighted sequences.

2 Multiparametric MRI (mp-MRI)

The first prostate MRI was performed in the mid-1980s (Steyn and Smith 1984). Ever since then, prostate MRI developed from a promising tool to a mature imaging modality, gathering not only morphological but also functional information. State-of-the-art mp-MRI preferably performed at 3 T nowadays includes T2- and T1-weighted imaging yielding morphological information as well as DWI, dynamic-contrast-enhanced perfusion (DCE-MRI), and MR spectroscopy (MRS) providing primarily functional information (Table 1).

Bowel motion artefacts can be reduced by administering an antiperistaltic agent such as butylscopolaminbromid. Patients should be instructed about the importance of not moving during image acquisition. An endorectal coil (ERC) is not an absolute requirement at either 1.5 T or 3 T anymore, but strongly recommended for imaging at 1.5 T (Beyersdorff et al. 2003). 3 T MRI scanners and the associated higher signal-to-noise ratio (SNR) provide excellent image quality without ERCs, which in turn translates generally in better patient acceptance. Phased-array coils with multiple receiving channels are currently used in standard clinical practice.

2.1 T2-Weighted Imaging

T2-weighted imaging (T2WI) can provide high spatial resolution and clear depiction of the zonal anatomy of the prostate and therefore is indispensable for PCa detection, localization, and accurate tumor staging. Anatomically, the prostate gland has four distinct glandular regions, the peripheral zone, central zone, transition zone, and the anterior fibromuscular zone.

A healthy peripheral zone has homogeneous high signal intensity (SI) on T2-weighted images, as it consists mostly of glandular structures. The central zone has variable amounts of inhomogeneous intermediate SI. Several studies in the late 1980s established that PCa in the peripheral zone is characterized by low T2 SI. This is due to unrestricted growing of cancer cells that do not preserve the glandular structure of the peripheral zone (Bezzi et al. 1988) (Fig. 1).

In the central and transition zone, an irregular low-SI area without capsule resembling an “erased charcoal” or a SI-disrespecting normal glandular structure, the capsule or the urethra is considered malignant. High-grade cancers usually have a lower SI than low-grade cancers (Wang et al. 2008).

Interpretation of T2WI includes the evaluation of all adjacent structures in the male pelvis, especially capsule, seminal vesicles, and posterior bladder wall for extraprostatic tumor invasion as well as for lymph nodes and bone structures regarding lymphogenic or haematogenic tumor spread.

Table 1 Landmark studies correlating imaging modalities with histopathological results

mp-MRI	Histopathological correlation	References
HR T2	Glandular morphology	Bezzi et al. (1988)
DWI	Gleason score	Turkbey et al. (2011)
DCE-MRI	Neoangiogenesis	Engelbrecht et al. (2003)
MRS	Cell metabolism	Costello and Franklin (1997)

Sensitivity and specificity for T2WI differ among studies, Turkbey et al. found a sensitivity of 42 % and specificity of 83 % across all prostatic regions (Turkbey et al. 2010).

One drawback of T2WI alone is the limited specificity of low-SI areas. Benign abnormalities such as chronic prostatitis, atrophy, scars, postirradiation or antihormonal treatment effects, hyperplasia, and postbiopsy hemorrhage may mimic a low-SI-resembling tumor tissue (Kirkham et al. 2006).

2.2 Diffusion-Weighted Imaging (DWI) and the Apparent Diffusion Coefficient (ADC)

DWI adds important information about cellular density on a tissue level to the morphological information from high-resolution T2WI.

DWI as noninvasive, functional MR technique quantifies the Brownian motion of water molecules within tissue. Thereby, it enables not only qualitative but also quantitative tumor assessment. Reduced water diffusion in PCa has been attributed to increased cellularity through uncontrolled tumor growth with a consecutive reduction of the extracellular space. Therefore, DWI primarily provides an important quantitative biophysical parameter that can be used to differentiate benign from malignant prostatic tissue that shows the typical pattern of high SI on images with high b-values and low SI on the ADC map (Hosseinzadeh and Schwarz 2004) (Fig. 2a, b).

DWI in combination with T2WI is not only clinically relevant for improved tumor detection and characterization, but also increasingly used for therapy monitoring before, during, and after treatment (Chenevert et al. 2002). There is evidence that DWI allows to reflect cellular changes in malignant tissue, especially under radiation (Song et al. 2010).

DWI acquisition parameters should be optimized according to the respective MR imaging system as well as to the magnetic field strength that is implemented. The acquisition of at least two different b-values, which specify the sensitivity

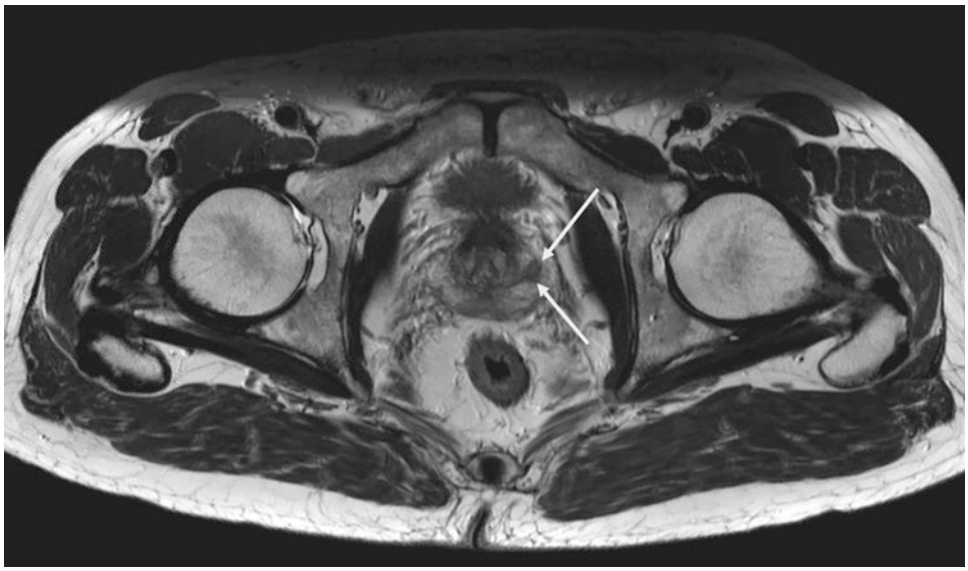

Fig. 1 Axial high resolution T2-weighted TSE showing a PCa lesion in the left peripheral zone (*white arrows*)

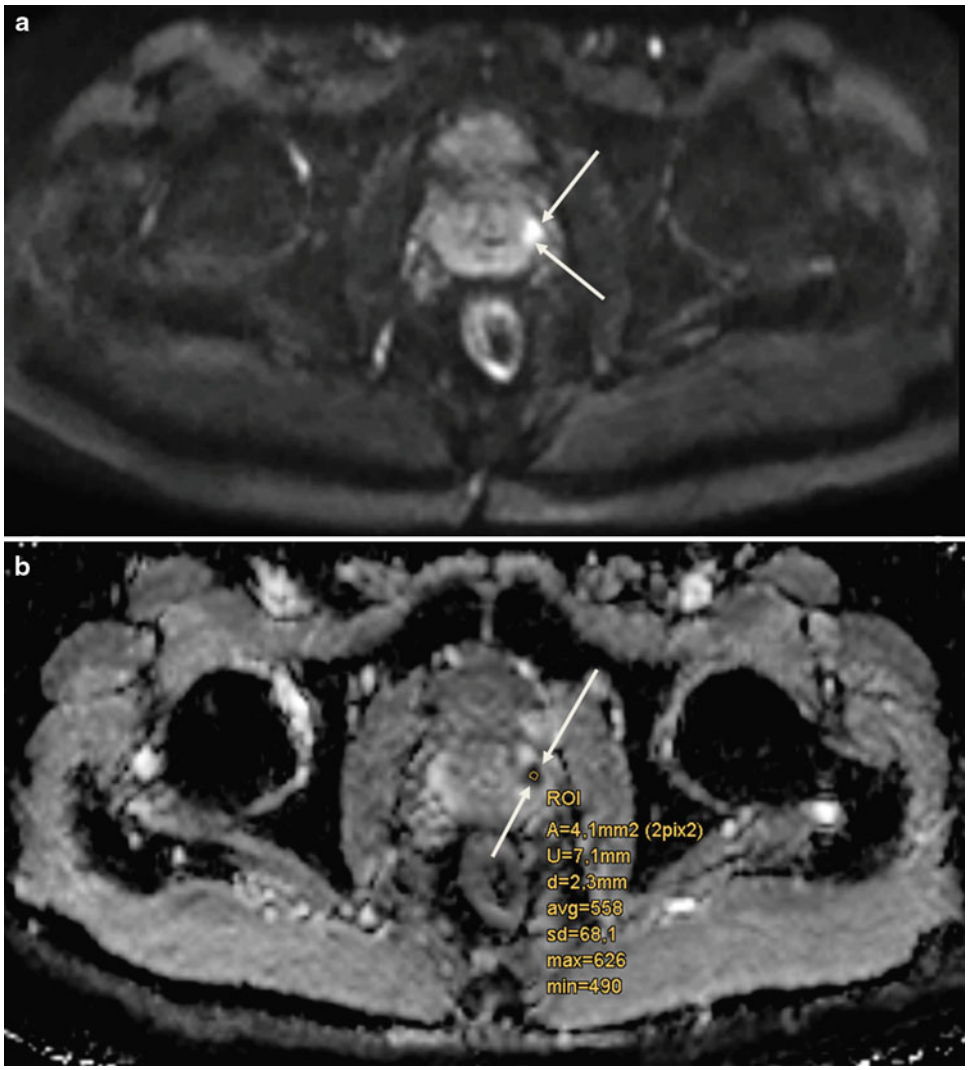

Fig. 2 **a** Axial DWI ($b = 800\ mm^2/s$) highlighting a PCa in the left peripheral zone (*white arrows*) and **b** corresponding axial ADC map

of diffusion weighting, is a prerequisite for the calculation of ADC maps for accurate quantitative analysis. Selection of the appropriate b-values for DWI is crucial because higher b-values increase the sensitivity to detect changes in diffusion, but at the same time impair the signal-to-noise ratio. Benefits of DWI are the relatively short acquisition time and high contrast resolution between tumors and normal tissue that is comparable to positron emission tomography (PET; "PET-like imaging"). A shortcoming of DWI is the vulnerability to susceptibility-induced distortion artefacts due to air/tissue interfaces, for example, at the boundary of the rectal wall.

DWI and the calculated apparent diffusion coefficient (ADC) in particular have initially been used to assess tumor aggressiveness, especially in brain cancers (Sugahara et al. 1999). In the meantime, several groups found out that ADCs obtained from DWI were significantly lower in PCas with higher Gleason scores (Turkbey et al. 2011). This allows for noninvasive assessment of the aggressiveness of PCas that are visible on MR images, which is an important predictor for patient outcome, prognosis, and can also be useful in the planning of radiation therapy.

2.3 Dynamic-Contrast-Enhanced MRI (DCE-MRI, Perfusion Imaging)

DCE-MRI is a functional imaging modality following the intravenous (i.v.) administration of gadolinium-based contrast medium allowing the characterization of pharmacokinetic features reflecting the prostatic vascularization through a series of high temporal resolution axial T1-weighted sequences.

Vascularization and angiogenesis in PCa are mostly induced through the secretion of vascular growth factors in reaction to the presence of local hypoxia or lack of nutrients due to uncontrolled fast growth of malignant cells (Bonekamp and Macura 2008). The resulting changes on a vascular level can be assessed dynamically by DCE-MRI. As the prostate gland is highly vascularized, a simple substraction of images before and after gadolinium administration i.v. is insufficient to properly delineate PCa, and a dynamic imaging series with adequate temporal resolution is required instead to accurately determine the time course of contrast media inflow and washout.

Tumor vessels are generally more permeable and disorganized than normal vessels. Because of the abundance of tumor vessels in PCa and the corresponding vessel walls' vulnerability and permeability, fast contrast arrival and rapid washout are typically observed (Fig. 3a, b). It has been demonstrated that the presence of washout is highly indicative for PCa (Alonzi et al. 2007), even in the absence of low SI in T2WI.

2.4 MR Spectroscopy of Prostate Cancer

2.4.1 ^{1}H-MR Spectrum and Metabolite Signals

While the morphologic and functional properties of normal or neoplastic tissue in the prostate gland can be delineated by MR imaging methods, in vivo proton MR spectroscopy (^{1}H-MRS) and spectroscopic imaging (^{1}H-MRSI) investigate its chemical composition noninvasively and thus yield further insight into prostate metabolism and the metabolic alterations caused by cancerous infiltration. Also, metabolic changes in the course of radiotherapy can be monitored, and the response of PCa to treatment may be assessed by MRS and MRSI. Of the metabolites present in the prostate gland, citrate (Cit), creatine/phosphocreatine (Cr), choline-containing compounds (Cho), and polyamines (PA) have sufficiently high tissue concentrations (above 1 mmol/kg) to be detected by MRS at the magnetic field strengths used for in vivo examinations. Cit is produced by oxidative phosphorylation within the citrate cycle and is extensively stored in healthy prostate tissue mainly in bound form as zinc citrate (Costello et al. 2005). It has a ^{1}H-MRS resonance at 2.65 ppm (chemical shift relative to tetramethylsilane as reference) arising from the non-equivalent methylene protons (CH_2) which are strongly coupled to form two almost overlapping spin doublets. This leads to a characteristic 4-peak spectral pattern at 3 T with two equally high central peaks spaced by 8 Hz and two smaller "outer" satellites each at 16 Hz distance (corresponding to the J coupling constant of Cit) from the central peaks. However, full resolution of all 4 peaks is achieved in vivo only with excellent magnetic field homogeneity, while in many prostate MRS acquisitions at 3 T, the two central constituents appear as a single broadened peak, which is a general issue at the lower field of 1.5 T. Also, the three methyl resonances of Cho, PA, and Cr covering the spectral range of 3.21–3.03 ppm are often not completely resolved, especially at 1.5 T, and therefore, usually the summed intensity (tChoCr) of all peaks in this frequency range is compared to the total area under the citrate components, yielding a metabolite ratio, e.g. called tChoCr/Cit.

Although being itself a complex overlay of several constituents such as glycerol phosphorylcholine (GPC), phosphorylcholine (PC), acetylcholine (ACho), and free choline, the intensity of the Cho peak centered at 3.21 ppm in the proton spectrum of prostate tissue may serve as a biomarker for the detection of malignant disease, just in analogy to the PSA value, with strongly increased Cho level or ratio Cho/Cit being suspicious for PCa (Cornel et al. 1993). As especially the phospholipids GPC and PC are key components released in cell membrane turnover, extensive cell proliferation as it is found in malignant tumors is often accompanied by a characteristic elevation of the choline peak in the ^{1}H-MR spectrum. Simultaneously, the accumulation of

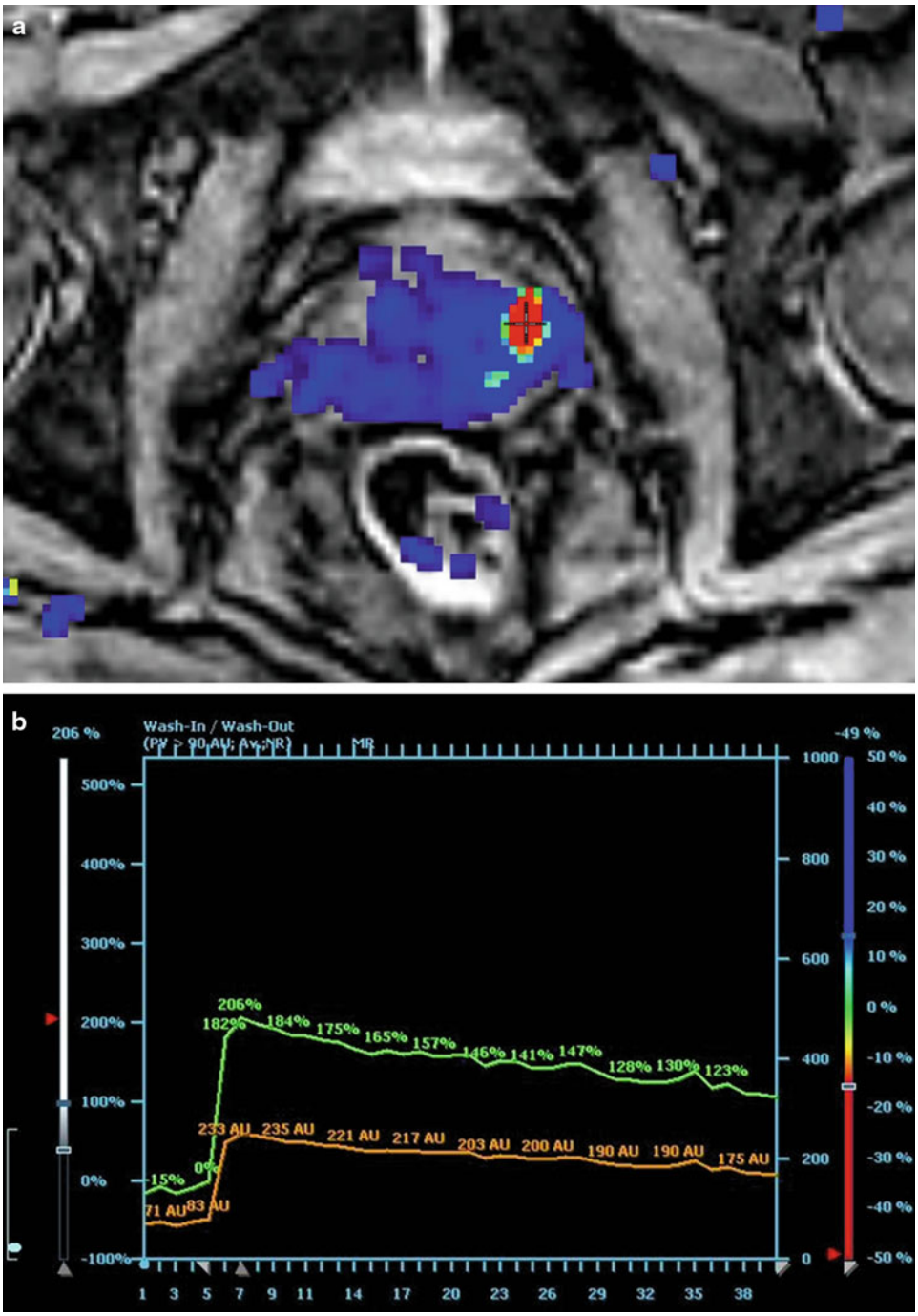

Fig. 3 **a** Axial high temporal resolution DCE-MRI with a PCa lesion in the left peripheral zone (*red spot*). **b** Corresponding enhancement curve with relative (*green curve*) and absolute (*orange curve*) depiction of contrast enhancement arrival and consecutive washout

citrate is inhibited in cancerous prostate tissue, and the MRS intensity of the citrate peaks decreases (Costello and Franklin 1997). Therefore, both effects add up to increase the metabolite ratio Cho/Cit. In contrast, the summed area tChoCr under the Cho, PA, and Cr spectral peaks and its ratio to Cit are less sensitive to indicate PCa, because an elevation in choline levels is at least partly counterbalanced by a reduction of Cr and PA in affected tissue. Nevertheless, in cases or at field strengths with insufficient spectral separation of Cho from the adjacent PA and Cr peaks, the tChoCr/Cit ratio may still serve as a suitable marker to discriminate between benign tissue and PCa, with values <0.8 being considered as normal and tChoCr/Cit >1 as highly suspicious for malignant disease. Correspondingly, a Cho/Cit ratio below 0.5 may indicate benign hyperplasia, while Cho/Cit ratio >0.6 suspects PCa, with borderline assignment for values in between (Crehange et al. 2011). However, such thresholds have to be regarded with care as they may vary depending on the used field strength, the scan parameters (mainly TR and TE) of the MRS acquisition sequence, and the achieved spectral peak

resolution. Moreover, the metabolite ratios differ between the prostate zones (with normal Cho/Cit being lower in the peripheral zone), and the cutoff values for discrimination between benign tissue and tumor have to be adjusted to the respective location within the gland.

While ^{1}H-MRS has been shown to be rather specific in the detection of PCa (89–91 % specificity), its sensitivity (75–77 %) is still inferior to other modalities (Manenti et al. 2006). One reason for missing a PCa lesion might be a too small or lacking increase of choline in tumors with only moderate cell proliferation, which is possibly associated with a lower Gleason score. Such a correlation between the Gleason score and the Cho levels in MRS has been found in some, but not in all studies (Zakian et al. 2005; Scheenen et al. 2007; Kobus et al. 2011). Also, PCa with focal size less than 1 cm is prone to be missed by MRS due to its limited spatial resolution, resulting in partial volume averaging with healthy tissue and thus yielding metabolite ratios below the chosen malignancy threshold. On the other hand, false-positive findings may be derived from high Cho signal also occurring in prostatitis, or if an intense narrow spectral peak is observed in MR spectra from the posterior parts in the basal region of the prostate, at the choline frequency of 3.2 ppm. This signal can be assigned to GPC contained in the seminal vesicles, and attention has to be paid not to mistake this "normal" GPC peak from seminal fluid with a pathological elevation of choline levels suspecting prostate cancer in that region.

2.4.2 ^{1}H-MRS Acquisition and Spatial Localization

The achievable spatial resolution for in vivo prostate MRS is one of the major drawbacks of this technique as the size of a tissue volume from which a proton MR spectrum is obtained by far exceeds the spatial dimensions of all other MR imaging methods and of most other imaging modalities. This is a consequence of the more than 10,000-fold lower tissue concentrations of the ^{1}H metabolites of interest (Cho, Cr, Cit) compared to the water protons used in MR imaging. Moreover, the intense spectral peak of water at 4.7 ppm has to be suppressed by suitable prepulses during MRS acquisition (and additionally by filtering algorithms in MRS postprocessing) to allow reliable quantification of the very small metabolite peaks, even when their chemical shift relative to water is quite large. Also, MRS signals from different molecular groups in lipids may overlay and distort the metabolite peaks, particularly of citrate, if the selected MRS volume partially includes fatty tissue. In localized single-volume (SV) ^{1}H-MRS, the metabolite signals are collected from within a brick-shaped tissue volume interactively placed on localizer MR images, which is selected by combining the excitation and refocusing RF pulses with magnetic field gradients for spatial encoding. This volume selection can be performed either with the point-resolved spectroscopy (PRESS) (Bottomley 1987) or the stimulated echo acquisition mode (STEAM) (Frahm et al. 1989) technique. Although the SNR of the metabolite peaks in the acquired MR spectra can strongly be improved by repeating the excitation of the volume of interest (VOI) and accumulating the MRS data ("signal averaging"), this may lead to unacceptably long measurement times if VOI sizes smaller than 2–3 cm^3 are desired, even at higher magnetic fields with their inherently better SNR. Therefore, in MRS of the prostate, SV techniques are not suited for accurate localization of a tumor within the tissue as the required VOI size would extend over a much too large part of the prostate gland. SV-MRS of prostate cancer might thus only be of interest if the tumor site is already known and the time course of progression or response to therapy is to be investigated in consecutive examinations.

2.4.3 MR Spectroscopic Imaging (MRSI)

By application of the MRSI technique (often also called chemical shift imaging (CSI)), a 2D or 3D grid consisting of a multitude of smaller voxels can be used to collect MR spectra from each of these voxels. To achieve this, similar to the principles of MR imaging, slice selection is performed by gradient switching during RF excitation, and additional phase encoding is applied for in-plane localization. In contrast to the MR imaging of water protons, however, it is not possible to use frequency encoding to acquire a complete row of the image following a single excitation, because the different frequency components of the detected MRS signal are already linked to the spectral information on the metabolites of interest. Therefore, phase encoding for two spatial directions (or even three in 3D-MRSI) has to be used, and as a consequence, m × n spin excitations spaced by the repetition time TR have to be performed to acquire the desired matrix of m × n MR spectra from all 2D grid voxels. Fortunately, the SNR in these spectra is not determined by the spin signal only from the corresponding small voxel, but from the total MRSI grid which above all is sampled m × n times and accumulated. In this way, in-plane voxel sizes around 1 cm^2 or below can be utilized with sufficient metabolite SNR in 2D-MRSI of the prostate, with typically 10 × 10–16 × 16 voxels over a grid extension of 8–12 cm. Because a field of view (FOV) of this size is completely surrounded by body tissue, back-folding of spin signal from outer structures would happen, like in MR imaging with such a small FOV, if only the 2D phase encoding was used for in-plane volume selection. Therefore, additional PRESS or STEAM localization of a VOI smaller than the margins of the phase-encoded FOV but completely covering the prostate gland has to be applied to avoid artificial signal contribution in the spectra of the MRSI voxels, especially from lipids. Suppression of such "outer volume" signals can also be achieved by multiple regional presaturation bars closely

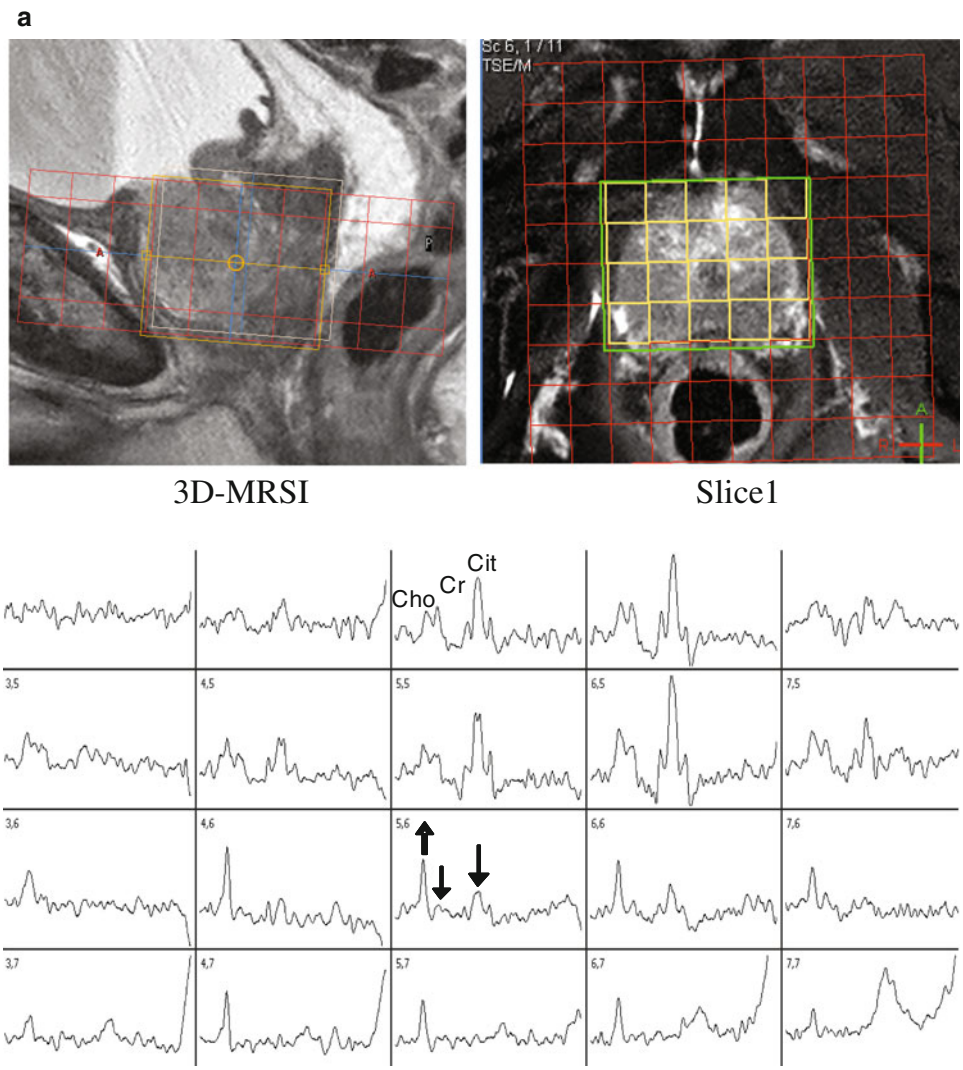

Fig. 4 3D-MRSI (TR/TE 1200/135 ms, acquisition matrix 10 × 10 × 3) of the prostate with external surface coil at 3T in a 74-year-old patient before radiotherapy. Overlay of MRSI grid (*red*) of isotropic 1-cm voxels and PRESS selection volume (*green frame*) on sagittal and transversal T2W MR images, and 2D array of selected MR spectra arranged corresponding to the yellow-framed voxels. **a** Spectra from MRSI slice #1 (at the prostate apex) show normal metabolite levels in the anterior part of the gland and demonstrate prostate cancer focused right posterior, indicated by strongly enlarged choline in association with barely detectable citrate (see up/*down arrows*). **b** Acquired (*red*) and fitted (*blue on green baseline*) spectra from 4 voxels in central MRSI slice (#2) show steep transition from unaffected area (*upper row*) to clearly malignant tissue (*lower row*) in directly adjacent voxels. Vertical scaling of spectra in (**b**) different from (**a**)

adapted to the individual prostate shape. In most cases, the cranio-caudal size of the prostate is too large to be entirely included in a 2D-MRSI acquisition with a slice thickness of 1–2 cm, and a 3D phase encoding scheme with at least three axial slices has to be used then. Fig. 4 shows an example for the image-guided planning of such a 3D-MRSI acquisition (TR/TE 1200/135 ms) with display of the 10 × 10 × 3 voxel grid (red), the PRESS-localized VOI (green frame), and a selection of spectra (yellow-framed voxels) from the peripheral and from the central zone of the prostate within the VOI. In this examination performed before radiotherapy, a high Cho peak and low Cit level indicating extensive tumorous infiltration are present in the spectra from the posterior region of the prostate, with accentuation in the right glandular lobe and apical. Just as the other techniques of multiparametric MR imaging, also MRS and MRSI of the prostate profit from the signal gain achievable by the use of an endorectal RF coil for signal detection, and its application allows to further decrease the minimum voxel size. While at magnetic fields of 2 T or less, the application of ERCs for prostate MRSI is mandatory, at 3 T the inherently higher MR signal and the stronger sensitivity to susceptibility artifacts caused by the endorectal placement might balance out the advantages of such coils. Therefore, also considering the signal increase gained by recent progress in MR detection sensitivity by digital RF chains and coil development, the sole use of external surface coils will at 3 T supply sufficient SNR and spatial resolution for MRSI, combined with more patient comfort.

Corresponding to the cutoff values for the metabolite ratios tChoCr/Cit and Cho/Cit cited before, but on a less stringent scale and thus more considering the dependency of such limits on the location within the prostate gland and on the MRS scan parameters, the new PI-RADS diagnostic grading of prostate lesions has been extended also to assessment by MRS (Barentsz et al. 2012). In the qualitative scoring of MRSI, only the peak heights for Cho and Cit are compared, from PI-RADS 5 corresponding to “Cho>>Cit,

Fig. 4 continued

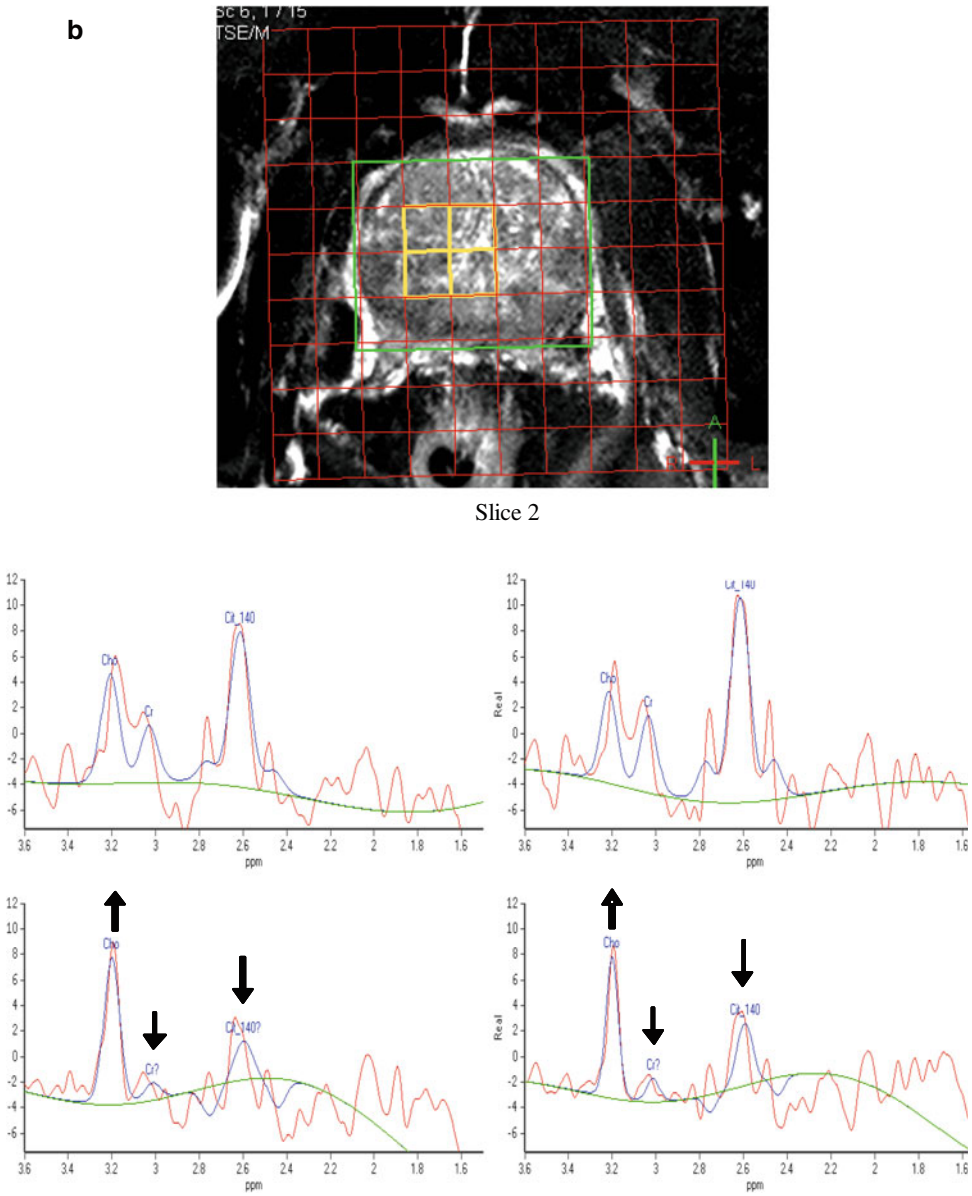

cancer is highly likely to be present" down to PI-RADS 1, assigned when "Cho<<Cit, disease is highly unlikely to be present."

2.4.4 MRSI of the Prostate in Radiotherapy Planning and Follow-Up

While the criteria described above can successfully be applied in the differential diagnosis between malignant disease and benign hyperplasia by MRS and in the localization of tissue with cancerous infiltration to define the target area in radiotherapy planning, a severe problem is encountered when response to therapy or residual/recurrent tumor has to be assessed by MRS in follow-up examinations after or during the course of radiation therapy: The citrate levels in irradiated prostate tissue are strongly decreased due to the metabolic damage induced by the radiation ["metabolic atrophy" (Pickett et al. 2004)], and recovery will not be achieved even years after the end of therapy. Therefore, all metabolite ratios with Cit as denominator will distinctly be elevated almost immediately after the first few radiotherapy fractions even when the tumor responds well and degrades in the course of irradiation. Figure 5 displays the typical alterations of metabolite levels in the course of radiotherapy in a case with prostate cancer located in the left central and peripheral zone, with very low amplitudes of all metabolite signals at therapy cessation demonstrating metabolic atrophy. A similar decline of the citrate levels (and corresponding increase of Cho/Cit and tChoCr/Cit) can also be seen in MRS already before radiotherapy in patients with adjuvant antihormonal therapy (Mueller-Lisse et al. 2007).

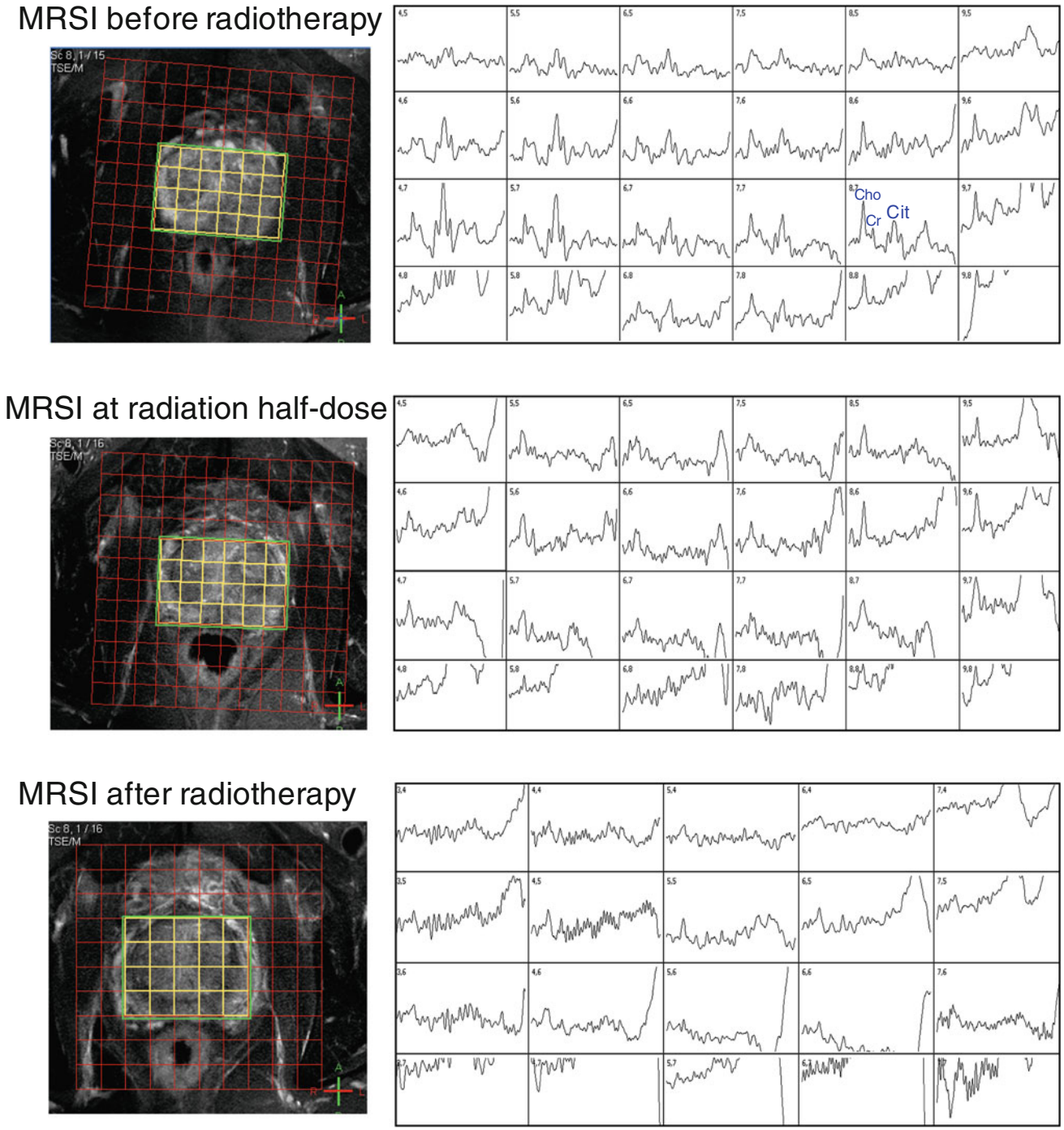

Fig. 5 MRSI at 3 T in the course of radiation therapy of prostate cancer in a 77-year-old patient. Display of MRSI grid and selected voxels within PRESS volume on fat-suppressed TSE and corresponding array of MR spectra acquired before the first therapy session (*upper row*), after reaching half of the total radiation dose (*middle row*) and shortly after the last therapy fraction (*lower row*). Initially, high Cho peak and reduced Cr and Cit signals in almost all spectra from the left glandular lobe indicate the cancerous infiltration. After reaching half of the total dose, citrate is no more detectable anywhere in prostate tissue, but Cho/Cr still remains elevated at the tumor location. In the examination after therapy, only very few MR spectra show metabolite signals above noise level, and this "metabolic atrophy" may be associated with a successful response to radiotherapy

As the ratios Cho/Cr or Cho/(Cr+PA) will not be affected that much by radiation-induced metabolic alterations, strongly increased values or even the mere identification of a distinct Cho peak in certain MRSI voxels may then serve as remaining indicators for tumor residue or recurrence (Westphalen et al. 2010). However, clear cutoff values for

these ratios cannot be defined easily, and due to general signal reduction of all metabolites in the course of radiotherapy, an artificial elevation in low-SNR spectra may also be observed. In addition, a final decrease in initially high values for Cho/Cr or Cho/(Cr+PA), indicating metabolic atrophy (and thus a successful response to radiotherapy), may be delayed even for months after therapy cessation. Therefore, in our experience, MR spectroscopy in the radiotherapy of prostate cancer should comprise an MRSI acquisition straight before the beginning of therapy (including antihormonal treatment) to assess tumor location and extension within the gland for a possible definition of target tissue for radiation boosts, and follow-up MRSI not before several months after therapy end to check for focal remaining or newly rising high choline levels. Nevertheless, the relevance of posttherapy choline and citrate levels in irradiated prostate tissue as prognostic factors for relapse-free survival or for tumor recurrence still remains a controversial issue and has to be investigated in further studies.

3 Summary

Multiparametric MR imaging and MR spectroscopy play a pivotal role in the assessment of prostate cancer. Current imaging should include morphology (T2-weighting), diffusion, perfusion, and spectroscopy, preferably at higher field strengths such as 3 T. State-of-the-art imaging allows for tumor detection, local tumor staging, and therapy monitoring. Future studies will provide even more evidence for the value of MR imaging and MR spectroscopy, especially in the context of therapy decision making.

References

Alonzi R, Padhani AR, Allen C (2007) Dynamic contrast enhanced MRI in prostate cancer. Eur J Radiol 63:335–350. doi:10.1016/j.ejrad.2007.06.028

Arumainayagam N, Ahmed HU, Moore CM et al (2013) Multiparametric MR imaging for detection of clinically significant prostate cancer: a validation cohort study with transperineal template prostate mapping as the reference standard. Radiology 268:761–769. doi:10.1148/radiol.13120641

Bains LJ, Studer UE, Froehlich JM et al (2014) Diffusion-weighted magnetic resonance imaging detects significant prostate cancer with a high probability: results of a prospective study with final pathology of prostates with and without cancer as the reference standard. J Urol. doi:10.1016/j.juro.2014.03.039

Barentsz JO, Richenberg J, Clements R et al (2012) ESUR prostate MR guidelines 2012. Eur Radiol 22:746–757. doi:10.1007/s00330-011-2377-y

Beyersdorff D, Darsow U, Stephan C et al (2003) MRI of prostate cancer using three different coil systems: image quality, tumor detection, and staging. RöFo Fortschritte Auf Dem Geb Röntgenstrahlen Nukl 175:799–805. doi:10.1055/s-2003-39929

Bezzi M, Kressel HY, Allen KS et al (1988) Prostatic carcinoma: staging with MR imaging at 1.5 T. Radiology 169:339–346. doi:10.1148/radiology.169.2.3174982

Bonekamp D, Macura KJ (2008) Dynamic contrast-enhanced magnetic resonance imaging in the evaluation of the prostate. Top Magn Reson Imaging TMRI 19:273–284. doi:10.1097/RMR.0b013e3181aacdc2

Bottomley PA (1987) Spatial localization in NMR spectroscopy in vivo. Ann N Y Acad Sci 508:333–348

Chang JH, Lim Joon D, Nguyen BT et al (2014) MRI scans significantly change target coverage decisions in radical radiotherapy for prostate cancer. J Med Imaging Radiat Oncol 58:237–243. doi:10.1111/1754-9485.12107

Chenevert TL, Meyer CR, Moffat BA et al (2002) Diffusion MRI: a new strategy for assessment of cancer therapeutic efficacy. Mol Imaging 1:336–343

Cornel EB, Smits GA, Oosterhof GO et al (1993) Characterization of human prostate cancer, benign prostatic hyperplasia and normal prostate by in vitro 1H and 31P magnetic resonance spectroscopy. J Urol 150:2019–2024

Costello LC, Franklin RB (1997) Citrate metabolism of normal and malignant prostate epithelial cells. Urology 50:3–12. doi:10.1016/S0090-4295(97)00124-6

Costello LC, Franklin RB, Feng P (2005) Mitochondrial function, zinc, and intermediary metabolism relationships in normal prostate and prostate cancer. Mitochondrion 5:143–153. doi:10.1016/j.mito.2005.02.001

Crehange G, Maingon P, Gauthier M et al (2011) Early choline levels from 3-tesla MR spectroscopy after exclusive radiation therapy in patients with clinically localized prostate cancer are predictive of plasmatic levels of PSA at 1 year. Int J Radiat Oncol Biol Phys 81:e407–413. doi:10.1016/j.ijrobp.2011.03.008

Delongchamps NB, Rouanne M, Flam T et al (2011) Multiparametric magnetic resonance imaging for the detection and localization of prostate cancer: combination of T2-weighted, dynamic contrast-enhanced and diffusion-weighted imaging. BJU Int 107:1411–1418. doi:10.1111/j.1464-410X.2010.09808.x

Djavan B, Ravery V, Zlotta A et al (2001) Prospective evaluation of prostate cancer detected on biopsies 1, 2, 3 and 4: when should we stop? J Urol 166:1679–1683

Dotan ZA (2008) Bone imaging in prostate cancer. Nat Clin Pract Urol 5:434–444. doi:10.1038/ncpuro1190

Engelbrecht MR, Huisman HJ, Laheij RJF et al (2003) Discrimination of prostate cancer from normal peripheral zone and central gland tissue by using dynamic contrast-enhanced MR imaging. Radiology 229:248–254. doi:10.1148/radiol.2291020200

Frahm J, Bruhn H, Gyngell ML et al (1989) Localized high-resolution proton NMR spectroscopy using stimulated echoes: initial applications to human brain in vivo. Magn Reson Med Off J Soc Magn Reson Med Soc Magn Reson Med 9:79–93

Hosseinzadeh K, Schwarz SD (2004) Endorectal diffusion-weighted imaging in prostate cancer to differentiate malignant and benign peripheral zone tissue. J Magn Reson Imaging JMRI 20:654–661. doi:10.1002/jmri.20159

Jeong IG, Lim JH, You D et al (2013) Incremental value of magnetic resonance imaging for clinically high risk prostate cancer in 922 radical prostatectomies. J Urol 190:2054–2060. doi:10.1016/j.juro.2013.06.035

Kim CK, Park BK, Lee HM (2009) Prediction of locally recurrent prostate cancer after radiation therapy: Incremental value of 3T diffusion-weighted MRI. J Magn Reson Imaging 29:391–397. doi:10.1002/jmri.21645

Kim JY, Kim SH, Kim YH et al (2014) Low-risk prostate cancer: the accuracy of multiparametric mr imaging for detection. Radiology 130801. doi: 10.1148/radiol.13130801

Kirkham APS, Emberton M, Allen C (2006) How good is MRI at detecting and characterising cancer within the prostate? Eur Urol 50:1163–1174; discussion 1175. doi: 10.1016/j.eururo.2006.06.025

Kobus T, Hambrock T, Hulsbergen-van de Kaa CA et al (2011) In vivo assessment of prostate cancer aggressiveness using magnetic resonance spectroscopic imaging at 3 T with an Endorectal coil. Eur Urol 60:1074–1080. doi:10.1016/j.eururo.2011.03.002

Lagemaat MW, Scheenen TWJ (2014) Role of high-field MR in studies of localized prostate cancer. NMR Biomed 27:67–79. doi:10.1002/nbm.2967

Manenti G, Squillaci E, Carlani M et al (2006) Magnetic resonance imaging of the prostate with spectroscopic imaging using a surface coil initial clinical experience. Radiol Med (Torino) 111:22–32

Mueller-Lisse UG, Swanson MG, Vigneron DB, Kurhanewicz J (2007) Magnetic resonance spectroscopy in patients with locally confined prostate cancer: association of prostatic citrate and metabolic atrophy with time on hormone deprivation therapy, PSA level, and biopsy Gleason score. Eur Radiol 17:371–378. doi:10.1007/s00330-006-0321-3

Noguchi M, Stamey TA, McNeal JE, Yemoto CM (2001) Relationship between systematic biopsies and histological features of 222 radical prostatectomy specimens: lack of prediction of tumor significance for men with nonpalpable prostate cancer. J Urol 166:104–109; discussion 109–110

Pickett B, Ten Haken RK, Kurhanewicz J et al (2004) Time to metabolic atrophy after permanent prostate seed implantation based on magnetic resonance spectroscopic imaging. Int J Radiat Oncol Biol Phys 59:665–673. doi:10.1016/j.ijrobp.2003.11.024

Roach M 3rd, Hanks G, Thames H Jr et al (2006) Defining biochemical failure following radiotherapy with or without hormonal therapy in men with clinically localized prostate cancer: recommendations of the RTOG-ASTRO phoenix consensus conference. Int J Radiat Oncol Biol Phys 65:965–974. doi:10.1016/j.ijrobp.2006.04.029

Romero Otero J, Garcia Gomez B, Campos Juanatey F, Touijer KA (2014) Prostate cancer biomarkers: an update. Urol Oncol. doi:10.1016/j.urolonc.2013.09.017

Scheenen TWJ, Heijmink SWTPJ, Roell SA et al (2007) Three-dimensional proton MR spectroscopy of human prostate at 3 T without Endorectal coil: feasibility. Radiology 245:507–516. doi:10.1148/radiol.2451061444

Song I, Kim CK, Park BK, Park W (2010) Assessment of response to radiotherapy for prostate cancer: value of diffusion-weighted MRI at 3 T. Am J Roentgenol 194:W477–W482. doi:10.2214/AJR.09.3557

Steyn JH, Smith FW (1984) Nuclear magnetic resonance (NMR) imaging of the prostate. Br J Urol 56:679–681

Sugahara T, Korogi Y, Kochi M et al (1999) Usefulness of diffusion-weighted MRI with echo-planar technique in the evaluation of cellularity in gliomas. J Magn Reson Imaging JMRI 9:53–60

Thompson IM, Pauler DK, Goodman PJ et al (2004) Prevalence of prostate cancer among men with a prostate-specific antigen level < or =4.0 ng per milliliter. N Engl J Med 350:2239–2246. doi:10.1056/NEJMoa031918

Turkbey B, Pinto PA, Mani H et al (2010) Prostate cancer: value of multiparametric MR imaging at 3 T for detection-histopathologic correlation. Radiology 255:89–99. doi:10.1148/radiol.09090475

Turkbey B, Shah VP, Pang Y et al (2011) Is apparent diffusion coefficient associated with clinical risk scores for prostate cancers that are visible on 3-T MR images? Radiology 258:488–495

Vicini FA, Vargas C, Abner A et al (2005) Limitations in the use of serum prostate specific antigen levels to monitor patients after treatment for prostate cancer. J Urol 173:1456–1462. doi:10.1097/01.ju.0000157323.55611.23

Wang L, Mazaheri Y, Zhang J et al (2008) Assessment of biologic aggressiveness of prostate cancer: correlation of MR signal intensity with Gleason grade after radical prostatectomy. Radiology 246:168–176. doi:10.1148/radiol.2461070057

Westphalen AC, Coakley FV, Roach M 3rd et al (2010) Locally recurrent prostate cancer after external beam radiation therapy: diagnostic performance of 1.5-T Endorectal MR imaging and MR spectroscopic imaging for detection. Radiology 256:485–492. doi:10.1148/radiol.10092314

Zakian KL, Sircar K, Hricak H et al (2005) Correlation of proton MR spectroscopic imaging with Gleason score based on step-section pathologic analysis after radical prostatectomy. Radiology 234:804–814. doi:10.1148/radiol.2343040363

PET/CT Imaging in Prostate Cancer: Indications and Perspectives for Radiation Therapy

H. C. Rischke and A. L. Grosu

Contents

Abstract

The goal of prostate cancer therapy is to administer risk-adjusted and patient-specific treatment with maximal cancer control and minimal side effects. Modern radiation techniques such as IMRT and IGRT for example enable application of high dose irradiation to the primary/dominant intraprostatic cancer lesions, to a local recurrent nodule after radical prostatectomy, or to the loco-regional lymph node metastases. Such approaches promise to offer significantly improved long term results but require most accurate imaging tools with the ability to reliably detect not only the primary tumor and nodal involvement but more importantly to precisely indicate their location and extent. In addition presence of distant disease should be reliably detected or excluded. In this review we present a detailed overview over numerous PET/CT-studies, with emphasis on choline-PET/CT, that investigated performance of PET/CT in different clinical scenarios, spanning from the initial presentation to PSA recurrent disease. We discuss benefits and limitations of this imaging device in the primary and salvage setting from the radio-oncologists point of view. In the situation of PSA recurrence, there is increasing evidence that in addition to local salvage RT of the prostate fossa after radical prostatectomy, salvage lymph node therapy seems feasible and advantageous for a significant proportion of patients. The accuracy of choline-PET/CT depends on absolute PSA level, PSA kinetics and the investigation depth level (e.g. lesion based vs. region based vs. patient based). Incorporation of metabolic information from Choline PET/CT or other forthcoming PET-tracers with similar or higher accuracy in the process of RT treatment volume definition appears beneficial for both primary and loco-regional recurrence, when lymph node therapy is indicated.

H. C. Rischke (✉) · A. L. Grosu
Department of Radiation Oncology,
Medical University of Freiburg, Robert Koch Str. 3,
79106 Freiburg, Germany
e-mail: hans.christian.rischke@uniklinik-freiburg.de

H. C. Rischke
Department of Nuclear Medicine,
Medical University of Freiburg, Hugstetter Str. 55,
79106 Freiburg, Germany

H. Geinitz et al. (eds.), *Radiotherapy in Prostate Cancer*, Medical Radiology. Radiation Oncology,
DOI: 10.1007/174_2014_1007, © Springer-Verlag Berlin Heidelberg 2014
Published Online: 11 May 2014

1 Introduction

Prostate Cancer (PCa) is currently second to lung cancer the leading cause of cancer death in men (Bernard et al. 2010; Strope and Andriole 2010), and is clinically a heterogeneous disease characterized by an overall long natural course in comparison to the other solid tumors, with a wide spectrum of biologic behavior that ranges from indolent to aggressive (Scher and Heller 2000). Though clinical nomograms based on prostate-specific antigen levels, Gleason score at biopsy and clinical stage at presentation have been developed for probability prediction of lymphatic spread, distant metastasis, and local recurrence (Heidenreich et al. 2008); diagnostic imaging modalities nowadays play an important clinical role in the management of PCa. Due to its biologically and clinically heterogeneous course and appearance evaluation and interpretation of imaging modalities is challenging.

PET/CT has been extensively explored to evaluate the extent of tumor spread both in the primary situation at initial diagnosis and in the state of biochemical recurrence to enable individual therapy concepts, and to assess treatment response (Kelloff et al. 2009).

Different radiotracers have been studied, such as carbon 11 (11C) and fluorine 18 (18F) labeled choline, acetate, and 18F-fluorodeoxyglucose, 18F-fluoro-5-alpha-dihydrotestosterone (18F-FDHT), 11C-methionine and others (Nunez et al. 2002; Albrecht et al. 2007; Dehdashti et al. 2005; Kotzerke et al. 2000; Larson et al. 2004; Toth et al. 2005). To reflect the use of radiopharmaceuticals from the clinicians view only those tracers that have already been evaluated in several clinical studies; and that are widely accepted and in clinical use are discussed in this chapter. 18F and 11C-choline are currently the most used tracer in this respect. Although several studies have evaluated 11C-acetate, 18F-fluorodeoxyglucose, and 18F-fluoride in PCa with interesting and promising results, their potential clinical benefit compared to labeled choline has not been entirely clarified in certain clinical settings. To elucidate the potential value of those tracers they are discussed additionally.

18F-labeled radiotracers, such as 18F-methylcholine or 18F-ethylcholine have a longer half-life than 11C-labeled radiotracers (110 min vs. 19 min). Despite the advantages of image properties of 11C-choline, the short half-life limits utility in the clinical situation as it must be prepared for each imaging study and cannot be transported off-site. 18F-choline can be used in institutions without an on-site cyclotron department and based on physicochemical properties; the short positron range of 18F results in higher spatial resolution and consecutively in better image quality (Bauman et al. 2012). Therefore, it is increasingly used in many institutions in Europe.

2 Radiotracers

2.1 11C-Choline, 18F-Choline

Choline is a quaternary ammonium compound used for phospholipid synthesis in cell membranes and transmembrane signaling (Lawrentschuk et al. 2006). Choline is incorporated into cells via the adenosine-triphosphate (ATP)-dependent choline transporter present in the cell membrane and then phosphorylated to phosphocholine by the choline kinase. Major mechanisms of phosphor-choline accumulation in tumor-cells are the malignancy-induced upregulation of choline kinase including enhanced choline transport, subsequent choline kinase-mediated phosphorylation, and activation of phosphatidylcholine-specific phospholipases (Iorio et al. 2010). Choline is an essential part of cell membrane phospholipids and therefore labeled choline derivates are "trapped" in the form of phosphatidylcholine (lecithin) in the tumor cell membrane (Pieterman et al. 2002; Jadvar 2011). The uptake of choline in tumor-tissue has been shown to be related to the rate of tumor cell proliferation (Bouchelouche et al. 2010). Biodistribution of 11C-choline and 18F-fluorcholine/18F-fluorethylcholine is different. 18F-choline has a longer half-life, but it is characterized by urinary excretion, that is negligible in 11C-choline, and therefore PET/CT-imaging with 18F-choline may interfere in pelvic imaging caused by high tracer accumulation in the bladder (Turkbey et al. 2009; Bouchelouche and Capala 2010). However, normal biodistribution of 18F/11C-choline demonstrates relatively high accumulation in the pancreas, liver, kidneys, and salivary glands, and variable uptake in the bowel (Fig. 1). Before presenting an overview of PET/CT technique and the available studies investigating the value of 11C/18F-choline PET/CT, we briefly discuss the other above-mentioned tracers and their potential.

2.2 11C-Acetate

Acetate is absorbed by cells and converted into acetyl-CoA. In this form, it can be involved into two different metabolic pathways: either anabolic or catabolic. Anabolic means that it can be used to synthesize cholesterol and fatty acids, thus forming cell membrane elements. Catabolic means that it can be oxidized in mitochondria by tricarboxylic acid cycle to CO_2 and H_2O, thus producing energy. Liu (2006) suggested that fatty acid metabolism, more than glycolysis, may be increased in PCa cells. Preclinical studies suggest an extensive involvement of the fatty acids synthesis pathway in acetate uptake in PCa and the upregulation of the key enzyme fatty acid synthase may play a role in genesis of prostate carcinomas (Vavere et al. 2008; Pflug et al. 2003).

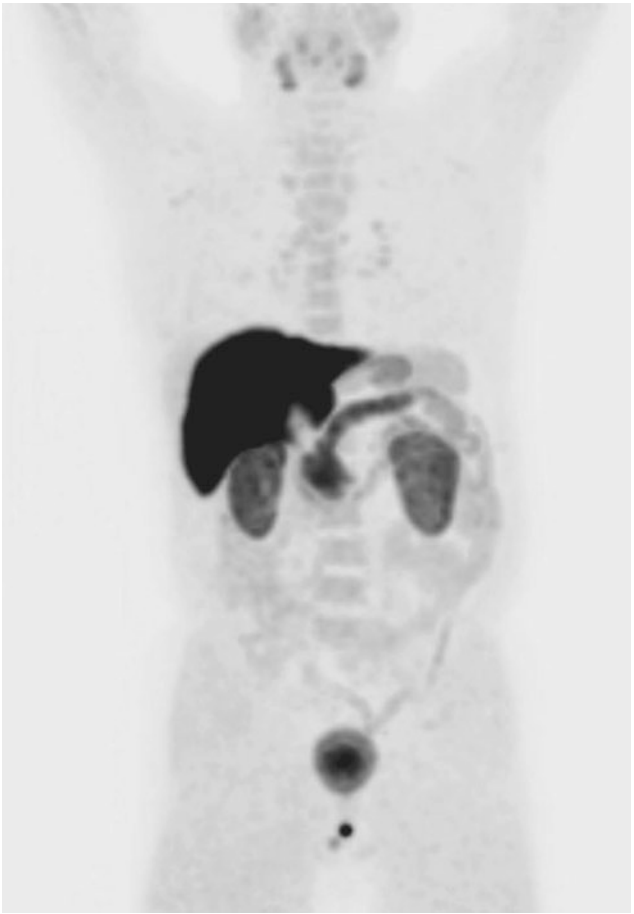

Fig. 1 Normal distribution of 18F-choline

Normal biodistribution of 11C-acetate demonstrates high accumulation in the pancreas, variable uptake in the liver and bowel, and some renal uptake, with little urinary excretion. Therefore, the elimination of 11C-acetate does not interfere with pelvic imaging (Seltzer et al. 2004; Fricke et al. 2003). In general, the biodistribution of 11C-acetate is very similar to 11C-choline. 11C-acetate, as well as the other below-discussed tracers, has been investigated for intra-prostatic primary tumor detection and staging as well as for re-staging of PCa in case of biochemical relapse. As with radiolabeled choline, the use of 11C-acetate for accurate detection of intra-prostatic cancer and the differentiation between cancer and normal prostatic tissue or benign hyperplasia is not feasible (Kato et al. 2002; Castellucci and Jadvar 2012). Kotzerke et al. (2002) found no significant difference between the use of 11C-acetate and 11C-choline in the detection of local recurrence after radical prostatectomy (RP), and Vees et al. (2007) found no significant difference between the detection rate of 11C-acetate and 18F-choline PET/CT. In summary, both 11C-acetate and 11C-choline appear to be equally useful in imaging PCa in individual patients, although more comparative data are eligible. In the era of 18F-choline with its advantage of a relatively long half-life, the potential of being used in centers without on-site cyclotron and at least being commercially available, it remains unclear if these studies will be performed ever. Recently, acetate labeled with a longer lived positron emitter, such as 18F, has been preliminary explored in preclinical studies (Ponde et al. 2007). But 18F-fluoroacetate is not a functional analog of 11C-acetate in normal physiology as it demonstrated prolonged blood retention, rapid clearance from liver, excretion in bile and urine, and high bone uptake due to defluorination (Lindhe et al. 2009). Its potential clinical use in PCa remains to be determined.

2.3 18F-Fluorodeoxyglucose (FDG)

Elevated glucose metabolism in malignant tissue in comparison with the normal tissue is based on increased expression of cellular membrane glucose transporters (Glut-1) and enhanced hexokinase II enzymatic activity in tumors (Gillies et al. 2008; Macheda et al. 2005; Smith 2000). PET-imaging with 18F-FDG, an analog of glucose, tracks the glucose metabolism of tissues. The integral role of FDG PET in oncology has been proven for many different tumors in different clinical situations. However, determination of the exact utility of FDG PET in PCa has not been defined so far and is still evolving (Jadvar 2011). FDG PET/CT showed a sensitivity of 80 % and a positive predictive value of 87 % for detection of prostate tumors with a Gleason score of 7 and greater in men who present with more than an intermediate risk of PCa based on elevated serum PSA level (Minamimoto et al. 2011). It appears that FDG PET may reflect the prostate tumor biology with more accumulation in more aggressive lesions that in less aggressive or indolent lesions (Castellucci and Jadvar 2012). 18F-FDG accumulation may overlap in normal prostate tissue, benign prostatic hyperplasia, and PCa tissues significantly, all of which often coexist (Salminen et al. 2002) and false-positive results may occur with prostatitis (Kao et al. 2008). 18F-FDG PET was less sensitive than 99m Tc-based bone scintigraphy at identifying bone metastases (Shreve et al. 1996). Compared to other tracers 18F-FDG PET/CT seems neither suitable in the diagnosis or loco-regional staging of clinically organ-confined disease nor in the detection of locally recurrent disease because of the relatively similar uptake of 18F-FDG by the post-therapy changes and malignant lesions and because of the high level of excreted radiotracer in the urinary bladder that may mask any lesions in adjacent tissues (Liu et al. 2001). FDG PET/CT may be particularly useful in men with advanced PCa (Fox et al. 2011) as it may distinguish metabolically active osseous lesions from metabolically dormant lesions (Morris et al. 2002). Other studies have also

shown a potential prognostic utility for FDG PET with generally higher tumor standardized uptake values (SUV) indicating poorer prognosis than those with lower SUVs, which is similar to the general experience with the other cancer types (Oyama et al. 2002; Meirelles et al. 2010). In summary, although FDG PET/CT is generally limited in the diagnosis and staging of clinically organ-confined disease, it may be able to reflect tumor aggressiveness, potentially detect disease sites in a fraction of men with high serum PSA level at the time of biochemical failure, and be useful in the objective assessment of response to chemotherapy or anti-androgen therapy, and in prognostication (Castellucci and Jadvar 2012).

2.4 18F-Fluoride

18F-Fluoride diffuses through bone capillaries into the bone extracellular fluid. Its plasma clearance is very rapid and its single-passage extraction efficiency is high. The fast blood clearance of 18F-fluoride provides an optimal target to background ratio. 18F-fluoride ions exchange with hydroxyl groups in the hydroxyapatite, at the surface of bone crystals, being particularly active at sites of bone remodeling with high turnover. Therefore, 18F-fluoride uptake represents osteoblastic activity in the neighborhood of osteoblastic, lytic, or marrow-based bone metastases (Jana and Blaufox 2006; Even-Sapir et al. 2007). Recent studies have shown good diagnostic performance of 18F-fluoride, resulting in a sensitivity of 89 % with a specificity of 91 %, but compared to 18F-choline there was no advantage; thus, the specificity of 96 % of 18F-choline was significantly higher with the same sensitivity (Langsteger et al. 2011). Also in the recurrence situation, 18F-fluoride was useful in the detection of occult metastases (Jadvar et al. 2012). Although 18F-fluoride-PET is widely considered superior to classical bone scintigraphy, no prospective studies have yet demonstrated an incremental benefit in staging or patient management. Further experience with 18F-PET/CT is required before it may replace conventional single photon bone scans, which are less expensive and more widely available (Bauman et al. 2012).

2.5 Other Tracers

Other tracers have been or are under current investigation. F18-FACBC (anti-1-amino-3-18F-fluorocyclobutane-1-carboxylic acid) is a synthetic l-leucine analog (Fox et al. 2012) and 11C-methionine is a radiolabeled amino acid. As an essential amino acid, L-methionine plays a central role in the altered metabolism of cancer cells, and the latter has been also studied extensively for brain tumor imaging (Grosu et al. 2005a, b, 2006, 2011); both tracers reflect increasing amino acid transport as a precondition for protein synthesis. 18F-FDHT (18F-fluoro-5α-dihydrotestosterone) tracks androgen receptor expression and reflects binding capacity (Liu et al. 1992); androgen receptors are upregulated in castrate resistant disease. 18F-3′-deoxy-3′-fluorothymidine (18F-FLT) tracks the thymidine salvage pathway of DNA (Bading and Shields 2008). Zr89-DFO-huJ591 is a monoclonal antibody to an epitope on extracellular domain of prostate-specific antigen (PSMA) promising for imaging and immunotherapy purposes (Fox et al. 2012; Pandit-Taskar et al. 2008). These radiotracers are able to visualize specific metabolic pathways or cell receptors. However, their use in the clinical context has not been clarified, thus requiring ongoing and future studies; their potential clinical benefit lies beyond the scope of this article.

3 Hardware and Technical Considerations

Integrated PET/CT imaging based on the intrinsic combination of PET and CT within a combined gantry adjustment results in the acquisition of complementary image information within a single examination protocol without the need to reposition the patient (Townsend 2008). The first PET/CT systems started in 2001, and since then staging and restaging of cancer patients has been improved significantly over stand-alone CT- and PET-data acquisition (Czernin et al. 2007; Thorwarth et al. 2012). Modern PET/CT systems for clinical use combine a whole-body, full ring PET and a multi-slice CT (Thorwarth et al. 2012; Lonsdale and Beyer 2010). Scintillation detectors (typically lutetium oxyorthosilicate (LSO)- or lutetium yttrium oxyorthosilicate (LYSO)-based detectors) are circularly arranged and provide a transverse field-of-view of 60–70 cm with measured isotropic image resolution of around 5 mm, but lesion detectability in PET is not only defined by the spatial resolution of the system, but also by lesion contrast. Thus, lesions that are smaller than the image resolution can still be detected in PET if the contrast between lesion and surrounding tissue is sufficiently high (Thorwarth et al. 2012).

The injected dose depends on the type of radiotracer and is usually in the range of about 3–5 MBq/kg. The uptake phase, the time span after tracer-injection, when the acquisition of the PET-data starts depends on the kind of tracer and on its half-life. Uptake times of 2–120 min are reported in literature (Bauman et al. 2012). For example, delayed imaging after injection of 18F-choline may improve the performance of 18F-choline PET for localizing malignant areas of the prostate, because studies have shown on dual-phase PET of the prostate, areas of malignancy consistently demonstrated stable or increasing 18F-fluorocholine uptake, whereas most areas containing benign tissue demonstrated